PERIDYNAMIC MODELING OF DYNAMIC BRITTLE FRACTURE IN A MULTI-LAYERED GLASS SYSTEM

Florin Bobaru[1], Youn Doh Ha[2]
University of Nebraska-Lincoln, Department of Mechanical and Materials Engineering
Lincoln, NE, 68588-0526, USA

ABSTRACT

Multi-layered brittle materials are of interest in designing novel advanced materials systems that perform better in the event of high-velocity impact or, more generally, are able to spread and redirect the shock waves energy better than single-layer systems. The difficulties in predicting the behavior of such systems at impact, using modeling and simulations in three-dimensions, have been insurmountable due to the lack of success of existing models in capturing with accuracy the fast dynamics of fracture and the damage evolution in brittle materials. The presence of interfaces complicates the problem. Recently, a new nonlocal model called peridynamics has been successfully used to model dynamic fracture in brittle materials. In this paper we develop a peridynamic model for a multi-layered glass system and obtain results for a high-velocity impact test for which experimental tests have been published in the literature. Most of the main features reported in the experiments are captured in the peridynamic results. The model is able to predict both diffuse damage zones, indicative of closely spaces cracks, and crevice cracks that develop in the system due to bending deformations. The peridynamic model uncovers the fascinating time-evolution of damage and the dynamic interaction between shock waves, propagating cracks, interfaces, and bending deformations in three-dimensions.

1. INTRODUCTION

Glass laminates have become important in recent years and several experimental studies have been dedicated to the behavior of these structures under dynamic loading ([1-3]). Experiments on high-velocity impact in multilayered glass structures find very complex damage patterns with significant differences between the layers. A complex material, glass [4], undergoes a variety of damage patterns under impact, including: crack branching (bifurcation of crack), crack-path instability and crack curving, successive branching events, circumferential or ripple cracking, micro-cracking, etc. The work published in [1] is a recent attempt of describing in detail the impact damage from a high-velocity projectile onto a glass multilaminate. The intention of the authors of [1] was to provide a platform for validation of analytical and numerical models for high-velocity impact onto glass laminates. The present contribution is a first attempt at numerically modeling the system used in [1] at the same scale, using a new mechanical model called peridynamics. While we employ the simplest peridynamic constitutive model for a generic brittle material, the results show that, to first order, we are able to obtain most of the structure of damage observed in the experiments. Future enhancements to the constitutive model could lead to quantitative predictive simulations using Peridynamics.

[1] corresponding author: fbobaru2@unl.edu
[2] current affiliation: Department of Naval Architecture, Kunsan National University, Korea.

The paper is organized as follow: in section 2 we briefly describe the peridynamic model and the computational details; in section 3 we give the peridynamic results and compare them with the experimental observations from [1]; conclusions are presented in section 4.

2. COMPUTATIONAL MODELING

2.1 The Peridynamic formulation

The peridynamic theory uses an integral of forces (per unit volume squared) acting at a point over a certain "horizon" (a nonlocal region around the point) instead of the divergence of stresses term in the classical equations of motion [5]. Since spatial differentiation is eliminated from the mathematical framework of peridynamics, this formulation is well suited for modeling problems in which displacement discontinuities emerge, interact, and evolve in time. The peridynamic equations of motion are:

$$\rho \ddot{u}(x,t) = \int_{H_x} f(u(\tilde{x},t) - u(x,t), \tilde{x} - x) dV_{\tilde{x}} + b(x,t)$$

where f is the pairwise force function in the peridynamic bond that connects point x to $\tilde{x}$, and u is the displacement vector field. ρ is the mass density and $b(x,t)$ is the body force acting at x at time t. The integral is defined over a region H_x called the "horizon" at point x. The region is taken here to be a circle of radius δ. Further comments about the horizon can be found in the literature (e.g. [6]).

These equations of motion are used with a linear micro-elastic material model [7] and a simple damage model as described in [8]. The computations in this paper are performed using EMU, a peridynamic code developed by Dr. S.A. Silling at Sandia. EMU uses a mid-point discretization scheme for the spatial integration. For the time-integration we use explicit integration (forward Euler) with a sufficiently small time-step to preserve numerical stability.

2.2 The Peridynamic model for the multi-layered glass system

A three-dimensional model of the multi-layered glass system is created using the geometry used in [1] and shown in Fig. 1. While the geometry of the seven-layer glass system with a polycarbonate backing is the same as in the experiments, the boundary conditions are slightly different from experiments. For example, in the experiments the impact face of the top layer is taped so that the fragments are not lost upon impact. The membrane effect induced by this certainly influences the mechanical response but whether this influence is of first or second-order remains to be seen. We do not impose conditions that mimic the taping of the front face. In addition, in the experiments the sides of the multi-layered system are also taped together. We, instead, enforce zero in-plane displacements for nodes on this boundary.

The simplest peridynamic linear-elastic with damage model is correlated to material properties for plate glass. The material properties for the glass material are: ρ=2440 kg/m^3, Young's modulus E=72GPa, and energy release rate G_0=135 J/m^2. The bond-based peridynamic model used in this work leads to a fixed Poisson ratio of 0.25 (in 3D), which is near that of the sodalime glass of 0.22. For the polycarbonate layer we used a density of 1200 kg/m^3 and Young's modulus

of 2 GPa. Since in the experiments no damage is observed in this layer, we chose a large critical relative elongation so that no damage is produced in the simulations either.

Also, in our simulations the polycarbonate layer has the same xy-dimensions as the glass plates and is fixed at the bottom, while in experiments the polycarbonate extends a little beyond the glass and there is supported only. The polycarbonate region directly under the glass is not supported. Because of this, and the absence of binding between the layers in the computational model, we do expect less damage in the results than is observed in the experiments. To get closer to the amount of damage seen in experiments, we select a slightly smaller system with 20 by 20 cm dimensions in the *xy*-plane, instead of the 30 by 30 cm used in experiments.

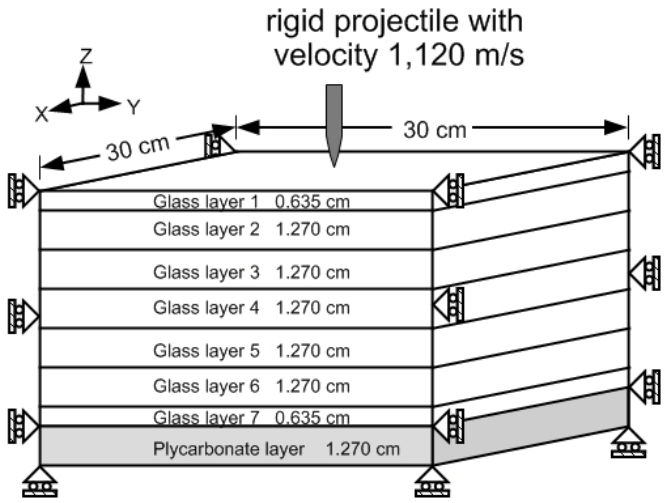

Fig. 1 The geometry and boundary conditions used in the peridynamic model.

A standard 12.7 mm, 13.4 g, projectile with an 18 mm long cylindrical body is used in the experiments with an initial velocity of 1,120 m/s. In the numerical simulations we use a rigid projectile of the same dimensions (ogive tip). Note that in the experiments, the projectile deforms from its 18mm initial length to 8mm after being ejected from the target.

In the experimental sample, the glass layers are bonded together with thin polyurethane layers which are not damaged, expect for that between the first and second layers punctured by the projectile. Polyurethane thin layer used in the experiments to bond the plates. Our current computational model does not include these thin layers since that would require more than one-billion degrees of freedom. We, instead, use simple non-penetrating contact conditions at the interfaces between the layers with no bonding.

The smallest horizon size we could compute with, based on the available computational systems, was around 2.4 mm, and the finest discretization we could afford used over 35 million degrees of freedom modeled for about 200 microseconds of real time. From the point of view of convergence for the damage patterns, and based on our convergence studies and previous work on dynamic crack propagation using peridynamics (see e.g. [9], [10]) we are near a converged solution. However, for obtaining crack propagation speeds close to those measured in dynamic brittle fracture, a sub-millimeter horizon size would have to be used. Such a horizon size,

coupled with a correspondingly finer grid, would also allow for capturing of damage details in the sub-millimeter range observed in experiments. Future plans include using such much larger models. Computations in this paper were performed on a multi-processor machine using up to 64 2.2GHz Opteron processors.

3. RESULTS

We briefly review the experimental results from [1] and then show the results obtained with the peridynamic model described above.

3.1 Experimental Results (from [1])

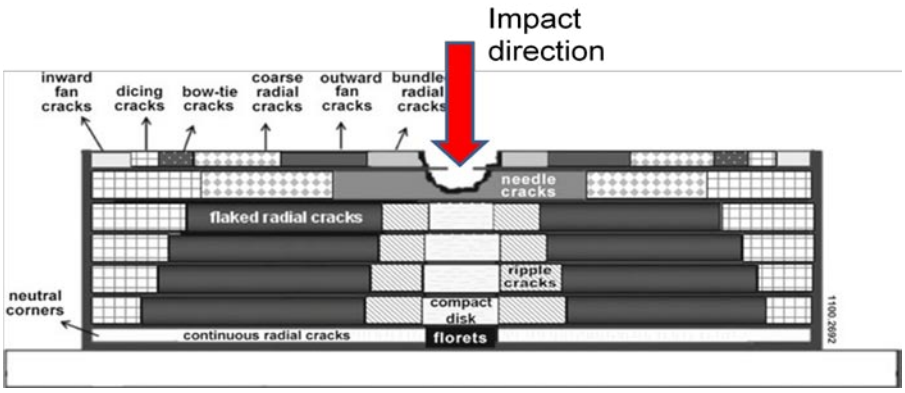

Fig. 1. Schematic of the types of cracks in a through-thickness cross-section (from [1]).

Bless and Chen [1] provide a careful and detailed description of the types of damage and cracks observed after the impact episode. The projectile stops in the second layer at a depth of 19 mm from the top surface and is ejected. No debonding between the glass and the polyurethane layers is observed and the polycarbonate support is not damaged. Because of the tape on the impact face, most of the fragments are recovered and a layer-by-layer study of the types of cracks observed indicates significant differences between the layers. The overall pattern of the damage zones is given in Fig. 1.

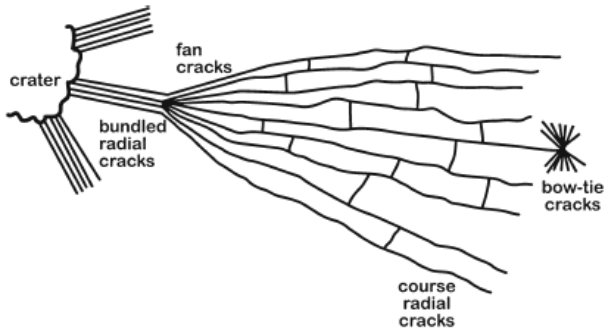

Fig. 2. Schematic of the types of cracks seen in experiments on the first layer (from [1]).

In the first layer the cracks emanate from the crated as bundled radial crack that fan, or branch, as they move away from the crater. The diagram shown in Fig. 2 is provided by the authors of

[1]. The outward fan cracks then become coarse and close to the boundaries dicing cracks and fine bow-tie cracks are also observed. In the second layer, near the central region closely spaced cracks (needle cracks) similar to dicing cracks but much finer, are observed. Individual needles measured around 1 × 1 × 20 mm.

The inner layers, from 3 through 6, were similar in appearance. Prominent ripple cracks near the center, then coarse radial cracks and dicing cracks near the boundaries. Quadrant cracks are a major feature in these layers, and Bless and Chen suggest that these are formed by bending/flexural deformation after the impact. This enforces the idea, also proposed in [11], that the impact layer fails in hoop tension whereas the inner layers fail by flexing. More transverse cracks were found in these inner layers than in the first two layers.

The last layer, the 7th, has the same thickness as the first one and featured a unique type of cracks: florets, which are small asterisk-like features located directly under the impact point. Bless and Chen [1] suggest that these features might be the base of conical fracture zones. Moving from the center to the boundaries, they observed florets, continuous radial cracks, and inward-fan cracks.

3.2 Peridynamic Simulation Results

We now present and examine the peridynamic results in terms of the damage index. The peridynamic index is computed at every discretization node and equals the number of broken peridynamic bonds divided by the total number of original bonds for that particular node. This definition means that the damage index is between zero and one and the legend shown in Fig. 3 is used in all the remaining pictures. A damage index of about 0.5 at points aligned along a thin line means that a crack separating two surfaces has been created. If, instead, the damage index map show no localization in an area, that means that diffuse-type damage has occurred the.

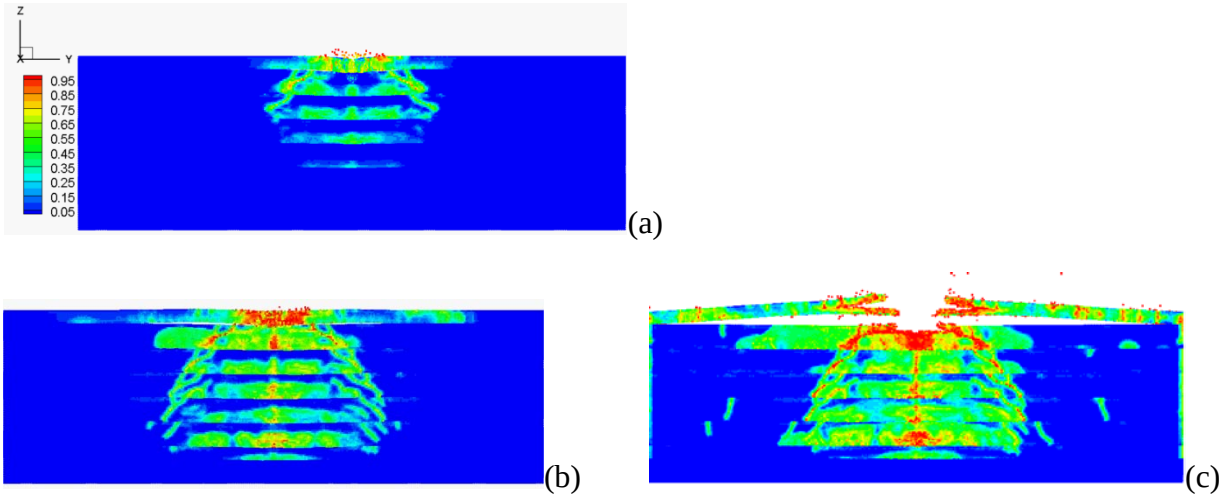

Fig.3 Time-evolution of the damage index maps for the middle through-thickness cross-section. Formation of the Hertz cone crack. Damage starts at the bottom of each layer and moves upward through-thickness mostly due to bending upwards.

In Fig. 3 the damage index map for a middle cross-section through the glass layers and the polycarbonate backing is shown as it progresses in time. We observe the formation of a Hertz cone crack similar to that described by the experiments in Fig. 1. Notice the time evolution of the cracks: in each layer, damage starts at the bottom of the layer and moves upward through-thickness mostly due to the bending upwards motion after the projectile has been ejected from the sample.

In our model we do not “glue” the glass layers together, therefore the first layer is flying away from the rest as a result of the flexural deformation of the entire structure. Notice also spall -type fractures in the cross-section of the first layer. The absence of the taping on the impact face in our model may contribute to that.

The projectile stops in the second layer, as in the experiments, at a depth of 16mm (compared to 19 mm in the experiments) and is ejected afterwards.

3.2.1 Damage evolution in the first layer

We observe that damage evolves differently between the top face and the bottom face of the first glass layer. The radial cracks start on the bottom face, they continue on both faces as bundled cracks that start to fan out as they propagate. This is very similar to the schematic description from the experiments of Bless and Chen [1].

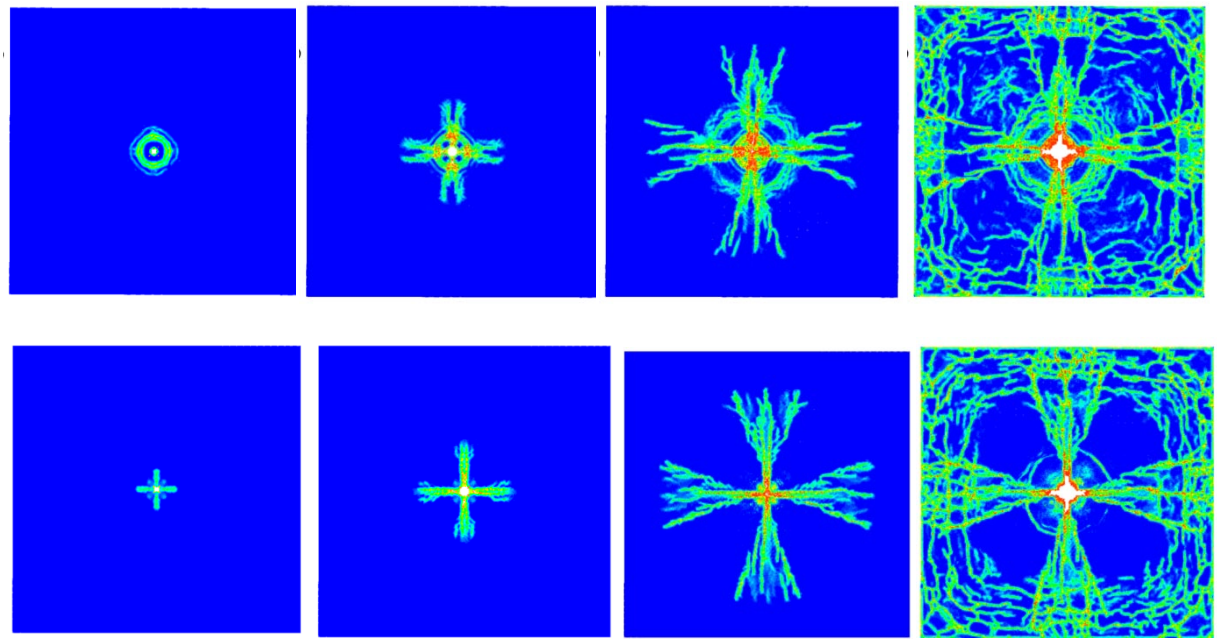

Fig. 4 Simulation results for the first layer at 7, 20, 36 and 90 μs, respectively from left to right. The top row shows the damage evolution as viewed from the top face of the layer, the bottom row shows the bottom face of the first layer.

Notice also that the “floret”-type crack on the bottom face is the same as that observed in [1] on the bottom of the last layer, and only seen there. We conclude that this type of crack is a result of the thickness of the layer. The peridynamic simulations demonstrates the presence of these

cracks only in the bottom faces of the first and last layers, which have half the thickness of the rest of the layers. Of course, the floret crack in the first layer is “erased” by the progression of the impact as the projectile perforates the first layer.

The cracks that have a similar location on the top and bottom faces are straight through-thickness cracks.

3.2.2 Damage patterns in the second layer

The second layer is suffering a very different type of damage compared with the first layer. The bundled radial cracks that fan out are not present; instead, a wider central region experiences a more diffuse-type damage (see Fig. 5). This type of damage may be indicative of the needle-type cracks observed in the experiments in this region. Note that the computational resolution we could afford at this time is not fine enough for obtaining fragments with dimensions of 1× 1 × 12 mm reported in the experiments.

In this second layer the projectile stops and is ejected from the target. In the computations, the projectile stops are around 16 mm from the surface, while in experiments the penetration depth reaches a similar value of 19 mm.

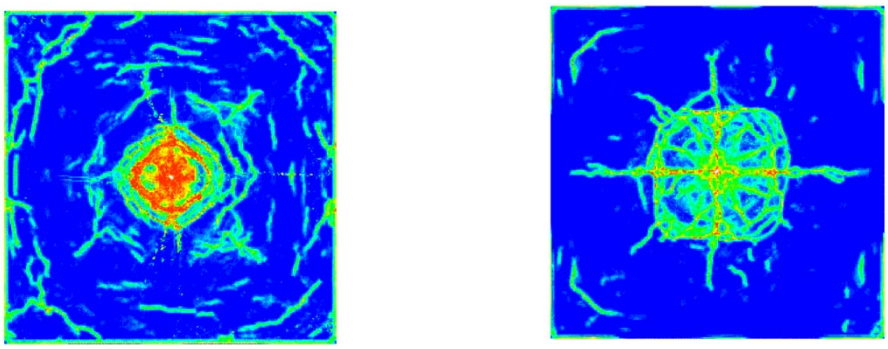

Fig. 5 Simulation results for the second layer at 80 μs. The top face (left) shows massive diffusive-type damage in the center region and a similar structure is seen on the bottom face but spread over a wider area. This may be indicative of the needle cracks seen in experiments.

The cone-type fracture through-thickness is becoming apparent here: notice the smaller damage area on the top face compared with the much wider on the bottom face. Radial cracks are more evolved on the bottom face, especially the quadrant cracks (vertical and horizontal, passing through the center) and they must be due to bending deformation.

3.2.3 Damage evolution in the inner (4th) layer

For the inner layers, 3rd to 6th, we select the 4th as a representative layer. Indeed, in the computational results as in the experiments, there is much similarity between the behaviors of these layers to the impact event. Fig. 6 contains the peridynamic results for the damage state at 80 μs. There is significant difference between how damage evolves in the top and bottom faces of this layer. Circumferential cracks (called ripple cracks in [1]) are highly prominent in the inner layers and they surround the central region, as reported in the experiments and schematically indicated by Fig. 1.

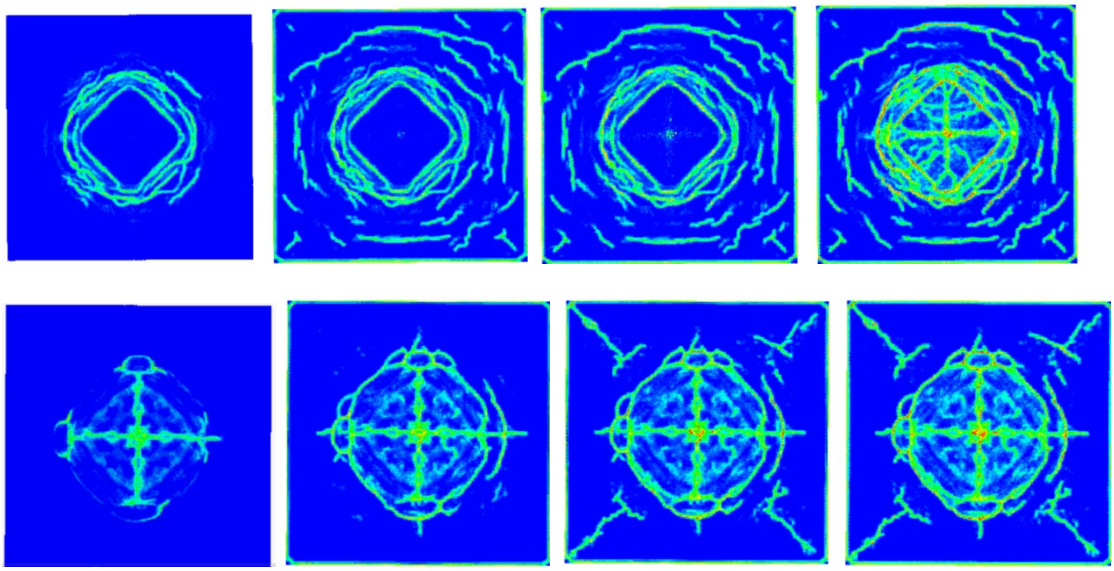

Fig. 6 Simulation results for the second layer at 40, 8, 120, and 210 μs. The top face (top row) shows significant ripple cracks, while on the bottom face damage starts with quadrant cracks (bottom row). The quadrant cracks become through-thickness cracks towards the end, due to the flexural bending motion.

Massive quadrant cracks (radial cracks along the horizontal and vertical directions, with the same symmetry as the structure) start on the bottom face and propagate, long after the projectile has been ejected, through the thickness as a results of flexural bending motion of the structure. These cracks are observed in the experiments as crevices and they propagate to the boundaries. In our simulations they appear to arrest when meeting some circumferential cracks. This difference may be due to different bending behavior caused by the absence, in our modeling, of the tape used in the experiments outside of the entire structure.

3.2.4 Damage evolution in the last (7th) layer

In the last layer of the multi-layered glass systems, which has the same thickness as the first one and half the thickness of the other layers, we observe the generation of the floret crack on the bottom face of the layer and ripple cracks on the top face. Interestingly, none of these are through-thickness cracks. The florets are reported in [1] including the fact that they are not through-thickness cracks.

We do not obtain the very straight radial cracks seen in experiments in this layer probably due to the zero-displacement conditions used on the backing. In experiments, there is no rear support to the polycarbonate directly behind the glass; the polycarbonate layer is supported over the area that extends outside the glass structure.

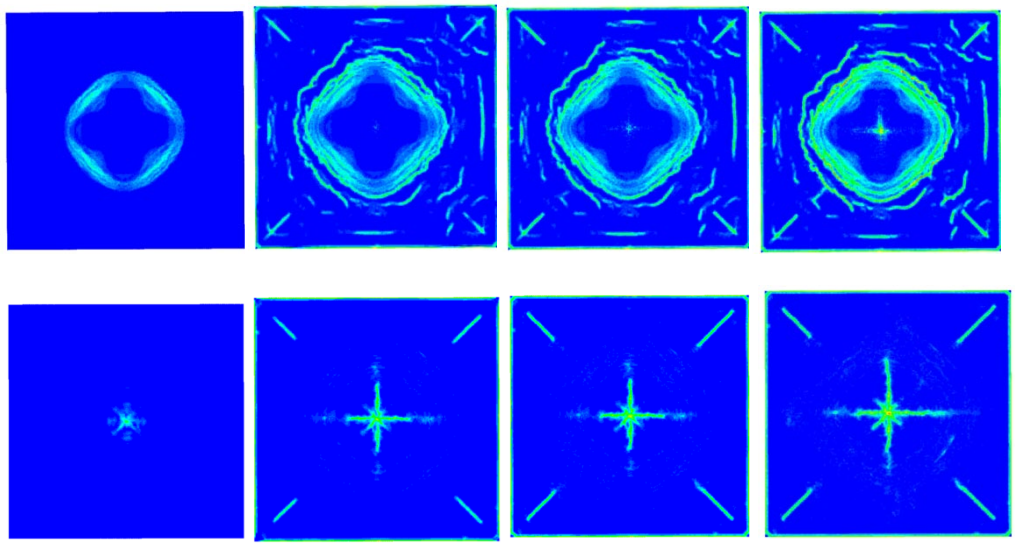

Fig. 7 Simulation results for the last (7th) layer at 40, 80, 120, and 210 μs. Most of the cracks here are not through-thickness cracks, except for the radial cracks coming from the corners. Observe the floret-type crack on the bottom face (bottom row) and the ripple cracks on the top face (top row).

4. CONCLUSIONS

The peridynamic model presented here showed that the dominant mechanisms that induce damage in the impact problem on a multi-layered brittle structure are: (a) the dynamics of stress waves and their interactions with the interfaces between layers, and (b) the structural response (flexural waves). The results show that linear-brittle peridynamic model is sufficient to roughly capture all fracture modes observed in the experiments. The computational simulations shed light on the time-evolution of damage, identifying when certain damage is initiated and the cause for it (expanding wave, reflected waves coming from the boundaries, flexural bending of the structure, etc). Finer features of damage observed in experiments, such as bow-tie cracks, needle cracks, are not captured, due to insufficient resolution in the numerical model. Compared with the experimental evidence, the computational results produced by peridynamics show more damage in the top layer and less in bottom layer. This behavior is likely due to the different conditions between the experiment and the boundary conditions we were able to impose computationally. For example, we do not tape the top face of the first layer, nor the layers together on their sides.

The peridynamic results presented here demonstrate that predictive simulations of dynamic fracture and damage in brittle materials are becoming a reality. With the understanding of how dynamic cracks move in these materials and how energy flows in structures where interfaces are present, the promise of one day being able to design novel materials is starting to move within reach in the near future.

4.1 Acknowledgements

The authors are thankful for the financial support offered through research contracts between UNL and the ARO (Dr. Larry Russell), and ARL (project coordinators Dr. C.F. Yen and Dr. C. Randow), ARO award number 58450EG.

5. REFERENCES

1. S. Bless and T. Chen (2010). Impact damage in layered glass. *International Journal of Fracture*, **162**(1):151–158, 2010.
2. P.J. Patel, G.A. Gilde, P.G. Dehmer, J.W. McCauley (2000). Transparent ceramics for armor and EM window applications. Proc SPIE 4102.
3. M.A. Grinfeld, J.W. McCauley, S.I. Schoenfeld, T.W. Wright (2007). Failure patterns in brittle ceramics and glasses. In: 23rd international symposium on ballistics, Tarragona, April16–20.
4. G.I. Kanel, S.J. Bless (2002). Compressive fracture of brittle solids under shock-wave loading. Ceramic armor materials by design. Ceram Trans 134:197–216.
5. S.A. Silling (2000). Reformulation of Elasticity Theory for Discontinuities and Long-Range Forces. Journal of the Mechanics and Physics of Solids 48: 175–209.
6. F. Bobaru, W. Hu (2012). The meaning, selection, and use of the peridynamic horizon. International Journal of Fracture (under review).
7. S. A. Silling, E. Askari (2005). A Meshfree Method Based on the Peridynamic Model of Solid Mechanics. Computers and Structures, 83: 1526-1535
8. S. A. Silling, F. Bobaru (2005). Peridynamic Modeling of Membranes and Fibers. International Journal of Non-Linear Mechanics, 40: 395-409.
9. YD. Ha, F. Bobaru (2010). Studies of dynamic crack propagation and crack branching with peridynamics. International Journal of Fracture, 162(1-2): 229-244.
10. YD. Ha, F. Bobaru (2011). Characteristics of dynamic brittle fracture captured with peridynamics. Engineering Fracture Mechanics, 78: 1156–1168.
11. X. Sun, A. Khaleel, R. Davies (2005). Modeling of stone-impact resistance of monolithic glass ply using continuum damage mechanics. International Journal for Damage Mechanics, 14: 165–178.